








# Backsplash galaxies and their impact on galaxy evolution: a three-stage, four-type perspective

Andrés N. Ruiz <sup>1,2\*</sup>, Héctor J. Martínez <sup>1,2</sup>, Valeria Coenda <sup>1,2</sup>, Hernán Muriel <sup>1,2</sup>,  
Sofía A. Cora <sup>3,4</sup>, Martín de los Ríos <sup>5,6</sup> and Cristian A. Vega-Martínez <sup>7,8</sup>

<sup>1</sup>*Instituto de Astronomía Teórica y Experimental (CONICET-UNC), Laprida 854, X5000BGR Córdoba, Argentina*

<sup>2</sup>*Observatorio Astronómico, Universidad Nacional de Córdoba, Laprida 854, X5000BGR Córdoba, Argentina*

<sup>3</sup>*Instituto de Astrofísica de La Plata (CONICET-UNLP), Observatorio Astronómico, Paseo del Bosque S/N, B1900FWA La Plata, Argentina*

<sup>4</sup>*Facultad de Ciencias Astronómicas y Geofísicas, Observatorio Astronómico, Universidad Nacional de La Plata, Paseo del Bosque S/N, B1900FWA La Plata, Argentina*

<sup>5</sup>*Departamento de Física Teórica, Universidad Autónoma de Madrid, E-28049 Madrid, Spain*

<sup>6</sup>*Instituto de Física Teórica, IFT-UAM/CSIC, Universidad Autónoma de Madrid, C/ Nicolás Cabrera 13–15, Cantoblanco, E-28049 Madrid, Spain*

<sup>7</sup>*Instituto Multidisciplinario de Investigación y Postgrado, Universidad de La Serena, Raúl Bitrán 1305, 1720256 La Serena, Chile*

<sup>8</sup>*Departamento de Astronomía, Universidad de La Serena, Av. Juan Cisternas 1200 Norte, 1720236 La Serena, Chile*

Accepted 2023 July 20. Received 2023 July 12; in original form 2023 June 1

## ABSTRACT

We study the population of backsplash galaxies at  $z = 0$  in the outskirts of massive, isolated clusters of galaxies taken from the MDPL2-SAG semi-analytical catalogue. We consider four types of backsplash galaxies according to whether they are forming stars or passive at three stages in their lifetimes: before entering the cluster, during their first incursion through the cluster, and after they exit the cluster. We analyse several geometric, dynamic, and astrophysical aspects of the four types at the three stages. Galaxies that form stars at all stages account for the majority of the backsplash population (58 per cent) and have stellar masses typically below  $M_{\star} \sim 3 \times 10^{10} h^{-1} M_{\odot}$  that avoid the innermost cluster's regions and are only mildly affected by it. In a similar mass range, galaxies that become passive after exiting the cluster (26 per cent) follow orbits characterized by small pericentric distance and a strong deflection by the cluster potential well while suffering a strong loss of both dark matter and gas content. Only a small fraction of our sample (4 per cent) becomes passive while orbiting inside the cluster. These galaxies have experienced heavy pre-processing and the cluster's tidal stripping and ram pressure provide the final blow to their star formation. Finally, galaxies that are passive before entering the cluster for the first time (12 per cent) are typically massive and are not affected significantly by the cluster. Using the bulge/total mass ratio as a proxy for morphology, we find that a single incursion through a cluster does not result in significant morphological changes in all four types.

**Key words:** methods: numerical – methods: statistical – galaxies: clusters: general – galaxies: evolution – galaxies: haloes – galaxies: kinematics and dynamics.

## 1 INTRODUCTION

For several decades, the study of galaxy clusters and their impact on the galaxy evolution has remained a captivating research subject. The process of galaxy evolution within clusters involves a myriad of physical mechanisms that operate across varying spatial and temporal scales. Both internal and environmental factors exert significant influence on the characteristics of galaxies, giving rise to a wide range of possible transformations and adaptations. Supernovae (e.g. Bower, Benson & Crain 2012; Stringer et al. 2012; Christensen et al. 2016), active nuclei (e.g. Nandra et al. 2007; Hasinger 2008; Silverman et al. 2008; Cimatti et al. 2013), and stellar feedback (e.g. Dalla Vecchia & Schaye 2008; Hopkins, Quataert & Murray 2012) are among the internal mechanisms that impact galaxies. On the other hand, properties of galaxies, such as star formation (e.g.

Hashimoto et al. 1998; Mateus & Sodré 2004; Welikala et al. 2008; Blanton & Moustakas 2009; Schaefer et al. 2017; Coenda et al. 2019), morphology (e.g. Dressler 1980; Whitmore, Gilmore & Jones 1993; Domínguez, Muriel & Lambas 2001; Weinmann et al. 2006; Bamford et al. 2009; Paulino-Afonso et al. 2019), luminosity (e.g. Adami, Biviano & Mazure 1998; Coenda et al. 2006), colour (e.g. Blanton et al. 2005; Martínez & Muriel 2006; Martínez, Coenda & Muriel 2008), and age (e.g. Thomas et al. 2005; Cooper et al. 2010; Zheng et al. 2017), are significantly influenced by their environment.

Several mechanisms impact galaxies in clusters, some of which cause gas depletion and the halt of star formation. Galaxies that move at high velocities through the intra-cluster medium (ICM) experience ram pressure stripping (RPS; e.g. Gunn & Gott 1972; Abadi, Moore & Bower 1999; Book & Benson 2010; Steinhauser, Schindler & Springel 2016), which removes a significant portion of their cold gas and reduces their star formation rate (SFR). Moreover, a galaxy's trip through the ICM can result in the removal of its warm gas, a phenomenon known as starvation (Larson, Tinsley &

\* E-mail: [andres.ruiz@unc.edu.ar](mailto:andres.ruiz@unc.edu.ar)

Caldwell 1980; McCarthy et al. 2008; Bekki 2009; Bahé et al. 2013; Vijayaraghavan & Ricker 2015). Starvation inhibits future star formation by cutting off the supply of gas that cools from the galaxy’s halo. Tidal stripping from the cluster potential is another mechanism that eliminates the gas supply (Zwicky 1951; Gnedin 2003a; Villalobos, De Lucia & Murante 2014). In contrast, in intermediate-density areas such as cluster outskirts and groups, harassment is a more effective galaxy–galaxy interaction mechanism (e.g. Moore et al. 1996; Moore, Lake & Katz 1998; Gnedin 2003b). It causes both gas depletion and morphological transformations. Tidal stripping from galaxy–galaxy encounters can truncate galaxies, mainly discs, and result in spheroid-dominated galaxies (e.g. Smith et al. 2015). Morphological evolution primarily depends on mergers (e.g. Toomre 1977; Barnes 1992; Di Matteo et al. 2007; Martin et al. 2018), with gas-rich minor mergers producing massive discs (Jackson et al. 2022), and with major mergers resulting in spheroidal systems (Navarro & White 1994).

Galaxies may encounter various environmental conditions and be subjected to one or more of the mechanisms discussed earlier at different stages of their life cycle. As galaxies fall towards clusters, they can experience different physical processes depending on whether they are part of a group (e.g. McGee et al. 2009; De Lucia et al. 2012; Wetzel et al. 2013; Hou, Parker & Harris 2014), falling from the field (e.g. Berrier et al. 2009), or falling through filament streams (e.g. Colberg et al. 1999; Ebeling, Barrett & Donovan 2004; Martínez, Muriel & Coenda 2016; Rost et al. 2020; Kuchner et al. 2022). Before entering the cluster, galaxies can undergo several physical transformations due to these processes, which are collectively called pre-processing (e.g. Fujita 2004; Mihos 2004).

After being incorporated into a cluster, galaxies have two possible outcomes: either they can remain bound to the cluster’s gravitational field or their trajectory can carry them away from the cluster, spanning distances of up to several  $R_{200}$ , the radius enclosing 200 times the mean density of the Universe (e.g. Mamon et al. 2004; Gill, Knebe & Gibson 2005; Rines & Diaferio 2006; Aguerri & Sánchez-Janssen 2010; Muriel & Coenda 2014; Casey et al. 2023). Eventually, these galaxies will turn around and fall back into the cluster during a subsequent infall. This unique population of galaxies is known as backsplash (BS) galaxies (Balogh, Navarro & Morris 2000). These particular galaxies can be used as laboratories to explore the impact of the cluster environment on galaxy properties, and to disentangle which stage is more important in their lifetimes. However, after these galaxies leave the cluster, they may show characteristics of ‘post-processing’ that are difficult to distinguish from ‘pre-processing’ signatures. In addition, observational studies have demonstrated that environmental effects may extend beyond the halo boundary to impact both baryonic components (e.g. Lu et al. 2012; Wetzel, Tinker & Conroy 2012) and dark matter haloes (e.g. Behroozi et al. 2014).

In the last few years, there have been many works about BS galaxies from a theoretical perspective. Benavides et al. (2021), using the ILLUSTRISTNG hydrodynamical simulations (Marinacci et al. 2018; Naiman et al. 2018; Nelson et al. 2018; Pillepich et al. 2018; Springel et al. 2018), have found that BS galaxies that were in the past satellite of another group or cluster can be the origin of quenched ultra-diffuse galaxies. Kuchner et al. (2022) explored the concept of BS galaxies that are falling into clusters along filaments. For the authors, these are galaxies outside the  $R_{200}$  that remain gravitationally bound to the cluster, and they may have made several orbits around the potential centre. The study reveals that between 30 and 60 per cent of filament galaxies are classified as BS galaxies. Interestingly, BS galaxies return to the cluster

after deviating significantly from their initial trajectory upon entry, particularly in more relaxed clusters. They do not exhibit a preferred location with respect to filaments and are unable to collapse and form filaments themselves. Several studies of BS galaxies around clusters have been carried out using THE THREE HUNDRED project (Cui et al. 2018), a suite of hydrodynamical resimulations of galaxy clusters. Haggar et al. (2020) found that the fraction of BS galaxies inhabiting a shell between  $R_{200}$  and  $2R_{200}$  varies from 21 to 85 per cent, with a mean value of 58 per cent, and that this fraction is dependent on the dynamical state of the cluster. Knebe et al. (2020) performed a detailed study of the shape and alignment of galaxies around clusters, finding that BS galaxies have a larger radial alignment and more spherical shapes than the infalling population of galaxies. Hough et al. (2023) discovered that approximately 65 per cent of quenched galaxies situated near clusters are BS galaxies. This suggests that a combination of RPS during the pre-processing stage and within the cluster is required to suppress star formation. Recently, Borrow et al. (2023) used ILLUSTRISTNG simulations to study BS galaxies around 1302 isolated galaxy clusters with mass  $10^{13.0} < M_{200}/M_{\odot} < 10^{15.5}$ . Their studies show that BS galaxies exhibit distinct characteristics compared to field galaxies, such as low gas fractions, high mass-to-light ratios, large stellar sizes, and low black hole occupation fractions.

The aim of this study is to investigate the existence and consequences of pre-processing in BS galaxies that have yet to cross the virial radius, as well as the effects of clusters on their subsequent evolution, once they are situated in the outskirts. Specifically, this research delves into the life cycle of these galaxies starting from 2 Gyr prior to their initial crossing of the virial radius. This paper is organized as follows. In Section 2, we describe the simulated galaxy catalogue and define the types and stages considered. Dynamical and astrophysical properties of BS galaxies are analysed in Sections 3 and 4, respectively. Finally, in Section 5 we present the main remarks of our work.

## 2 DATA

To construct our sample of simulated galaxy clusters, we have combined dark matter-only simulations of regions that contain cluster-like haloes at  $z = 0$  taken from the MDPL2 cosmological simulation, along with the semi-analytical model of galaxy formation SAG. In this regard, we will first provide a brief overview of the dark matter simulation and the semi-analytical model, followed by a description of the selection criteria employed to construct the galaxy sample in and around clusters.

### 2.1 The MDPL2 cosmological simulation

The MDPL2 cosmological simulation is one of several simulations within the MULTIDARK suite (Riebe et al. 2013; Klypin et al. 2016). This simulation contains  $3840^3$  dark matter particles in a comoving cubic box measuring  $1 h^{-1}$  Gpc in length on each side. Each particle has a mass of  $m_p = 1.51 \times 10^9 h^{-1} M_{\odot}$ . The simulation assumes a flat Lambda cold dark matter cosmology with  $\Omega_m = 0.307$ ,  $h = 0.678$ ,  $n = 0.96$ , and  $\sigma_8 = 0.823$ , which is consistent with measurements made by Planck Collaboration XVI (2014) and Planck Collaboration XIII (2016). Using GADGET-2 (Springel 2005), the simulation tracks the dynamical evolution of dark matter particles from an initial redshift  $z = 120$ . Over the course of the simulation, 126 snapshots were recorded between redshifts  $z = 17$  and  $z = 0$ .

Dark matter haloes and subhaloes were identified using the ROCKSTAR phase-space halo finder (Behroozi, Wechsler & Wu 2013a), and

merger trees were constructed using CONSISTENTTREES (Behroozi et al. 2013b). The halo/subhalo catalogues and merger trees used in this study are publicly accessible through the CosmoSim<sup>1</sup> and Skies & Universes<sup>2</sup> data bases, and form the foundation of the semi-analytical model for generating the galaxy population.

## 2.2 The SAG model

The semi-analytical model of galaxy formation and evolution SAG (acronym for semi-analytical galaxies) has its roots in the model presented by Springel et al. (2001); the most recent version is described in Cora et al. (2018). It simulates the formation and growth of galaxies within each detected dark matter halo, tracking the evolution of galaxy properties through the merger trees of haloes and subhaloes. The model can be used to study a wide range of galaxy properties, including their luminosity functions, mass functions, star formation histories, and morphologies. The SAG model incorporates physical processes such as gas cooling, star formation, and chemical enrichment. Star formation proceeds in both quiescent and bursty modes; the former takes place in gaseous discs, and the latter is triggered by disc instabilities and mergers contributing to the formation of a stellar bulge and the growth of a central supermassive black hole. Feedback processes from both supernovae and active galactic nuclei are also included.

One of the key strengths of the SAG model is its ability to incorporate environmental effects, such as RPS and tidal stripping, on galaxy properties. These effects occur predominantly within groups and clusters, which is particularly relevant to the current investigation. Upon becoming satellites, galaxies retain a hot gas halo that is gradually removed by various processes, with RPS being the primary contributor. As a result, the hot gas halo of a satellite galaxy serves as a protective barrier against the effects of the ram pressure exerted by the intra-group/intra-cluster medium on the cold gas located within the galaxy's disc. This protective function persists provided that the ratio between the hot gas halo and the galaxy's baryonic mass is greater than 0.1. None the less, if this ratio drops below the aforementioned threshold, the hot gas halo is considered exhausted, which enables ram pressure to strip the cold gas disc. The application of RPS relies on a novel analytical fitting profile, which simulates the force of ram pressure acting upon satellite galaxies in distinct environments (characterized by the dark matter halo mass), at different halocentric distances and redshifts (Vega-Martínez et al. 2022).

The SAG model accounts for orphan galaxies by monitoring satellites left over from haloes that the underlying simulation can no longer resolve. It uses the information provided by an orbital evolution model that encompasses both dynamical friction and mass-loss by tidal stripping (Delfino et al. 2022). Although the calibration of the model, that is, the fine adjustment of the free parameters associated with certain implemented physical processes, takes orphan satellites into account, they are not included in the sample analysed in this study.

The calibration is accomplished by utilizing the Particle Swarm Optimization technique (Ruiz et al. 2015), which yields a set of best-fitting values for the free parameters by comparing the model results against a given set of observables. The galaxy properties considered for calibration include the stellar mass functions at redshifts  $z = 0$  and  $z = 2$ , the distribution function of SFRs at  $z = 0.15$ , the percentage of

cold gas mass as a function of stellar mass at  $z = 0$ , and the correlation between bulge mass and the mass of the central supermassive black hole at  $z = 0$ . Table 1 in Cora et al. (2018) displays the values of the free parameters defining the model version utilized in this study, with the exception of the parameter responsible for regulating the redshift dependence of the reheated and ejected cold gas by supernova feedback (parameter  $\beta$ ; see their equations 10 and 12). This parameter has been reduced to enhance the agreement between the simulated and observed values of the evolution of the SFR density and the fraction of quenched galaxies as a function of stellar and halo mass, which are predictions of the model (see, respectively, their figs 6 and 11). During the calibration process, the fit to the stellar mass function at  $z = 2$  results in  $\beta = 1.99$ , which favours larger supernova feedback efficiency at higher redshifts and, consequently, a reduction of the star formation activity at those redshifts; this activity is shifted to later epochs and  $z = 0$  galaxies have less time to be quenched. A better agreement between the aforementioned model predictions and observational data is obtained by fixing  $\beta = 1.3$  while keeping the rest of the parameter values from the calibration process, at the expense of predicting a higher number density of low-mass galaxies in the stellar mass function at  $z = 2$ . This smaller value of  $\beta$  is provided by the FIRE hydrodynamical simulations of Muratov et al. (2015), which guided the current implementation of supernova feedback in SAG.

## 2.3 The sample of simulated backsplash galaxies: three stages and four types

Our study focuses on 34 massive, relaxed, and isolated galaxy clusters that were selected from the MDPL2-SAG galaxy catalogue. To identify these clusters, we first applied selection criteria based on the halo mass and the presence of nearby companion haloes. Specifically, we selected all haloes at redshift  $z = 0$  with a mass  $M_{200} \geq 10^{15} h^{-1} M_{\odot}$ , and with no companion haloes within  $5 \times R_{200}$  that are more massive than  $0.1 \times M_{200}$ . Here,  $M_{200}$  refers to the mass enclosed within a region of radius  $R_{200}$  that encompasses 200 times the critical density. These selection criteria were designed to exclude haloes that are undergoing major mergers or interacting with massive companions, which may have an impact on the orbits of galaxies in the vicinity of the clusters. This cluster sample is identical to the one employed in the works of de los Rios et al. (2021) and Coenda et al. (2022) for the development and testing of the ROGER code, which dynamically classifies galaxies in and around clusters in the projected phase space. Throughout this paper, we use galaxies with  $M_{*} \geq 3 \times 10^8 h^{-1} M_{\odot}$  since stellar mass functions and galaxy properties cannot be reliably replicated for galaxy masses lower than this threshold (Knebe et al. 2018).

We have adopted the same classification scheme as de los Rios et al. (2021) to categorize galaxies in and around the selected clusters based on their orbits. In particular, we define BS galaxies as those galaxies which at  $z = 0$  are found outside  $R_{200}$ , having crossed this radius exactly twice in their lifetimes, the first time on their way in, and the second on their way out of the cluster.

Hereafter, our paper will solely focus on the backsplash galaxies, and we will refer to them as BS galaxies to prevent confusion with the term *backsplash stage*, introduced below.

We follow the evolution of galaxies through three stages in their lifetimes:

- (i) **Incoming stage:** the period of 2 Gyr preceding the first time a galaxy crosses  $R_{200}$  in an inward direction.
- (ii) **Diving stage:** the span of time the galaxy remains within  $R_{200}$ .

<sup>1</sup><https://www.cosmosim.org/cms/simulations/mdpl2/>

<sup>2</sup><http://skiesanduniverses.org/Simulations/MultiDark/>

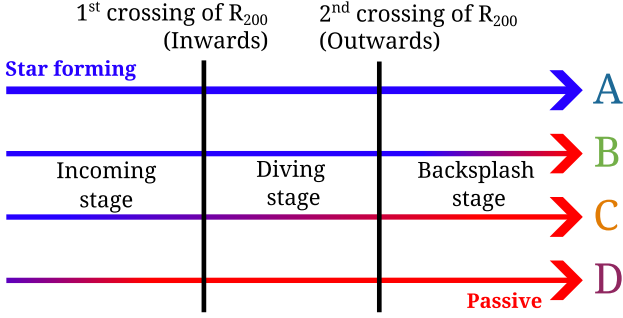


**Figure 1.** Scheme adopted for the selection of different types of BS galaxies based on the moment when a galaxy transitions from being star forming to a passive state. Blue colour symbolizes a star-forming galaxy, while red denotes a passive one. The four types of galaxies are as follows: galaxies that never become passive (A); galaxies that become passive during their backsplash stage (B); galaxies that become passive while they are inside the cluster (C); and galaxies that become passive before entering the cluster (D).

(iii) **Backsplash stage:** the lapse of time between the moment when the galaxy crosses  $R_{200}$  for the second time in an outward direction and the present epoch at  $z = 0$ .

Following the criterion adopted by Cora et al. (2018), galaxies with a specific star formation rate (sSFR) higher than  $10^{-10.7} \text{ yr}^{-1}$  are defined as star forming, meanwhile galaxies with sSFR below that threshold are classified as passive. We have classified the galaxies into four distinct types based on whether they are star forming or passive at the different stages.

(i) **Type A:** galaxies that are star forming throughout the three stages; 3038 galaxies in total, 58 per cent of the sample.

(ii) **Type B:** galaxies that become passive during their backsplash stage; 1353 galaxies, 26 per cent of the sample.

(iii) **Type C:** galaxies that become passive during their diving stage; 200 galaxies, 4 per cent of the sample.

(iv) **Type D:** galaxies that become passive prior to their diving stage, i.e. during the incoming stage or even before; 622 galaxies, 12 per cent of the sample.

This classification scheme is summarized in Fig. 1.

In Fig. 2, we show both the stellar mass distributions for the four types and for the total sample of BS galaxies at  $z = 0$  (upper panel), and the fraction of galaxies of each type as a function of their stellar mass at  $z = 0$  (bottom panel). There is no surprise in this plot. At the low-mass end ( $M_* \lesssim 10^{10} h^{-1} M_\odot$ ), the majority of galaxies are still star forming (type A). The fractions that follow in descending order correspond to galaxies that ceased star formation after leaving the cluster (type B). On the other hand, at the high-mass end ( $M_* \gtrsim 10^{11} h^{-1} M_\odot$ ), most of the galaxies were passive prior to diving into the cluster (type D). The transition between these two regimes occurs at intermediate masses,  $M_* \sim 3 \times 10^{10} h^{-1} M_\odot$ . The fraction of galaxies that became passive during their diving stage (type C) is very low over the whole range of mass, accounting only for 4 per cent of the complete sample of galaxies. This is an indication that the cluster environment cannot easily quench a galaxy while diving through it for the first time. Nevertheless, about a quarter of all BS galaxies ( $\sim 30$  per cent of the galaxies that entered as star forming) become passive after leaving the cluster (type B), which suggests that the effects of the cluster environment on the star formation of galaxies are not immediate and may take some time to manifest. Galaxies with stellar masses below

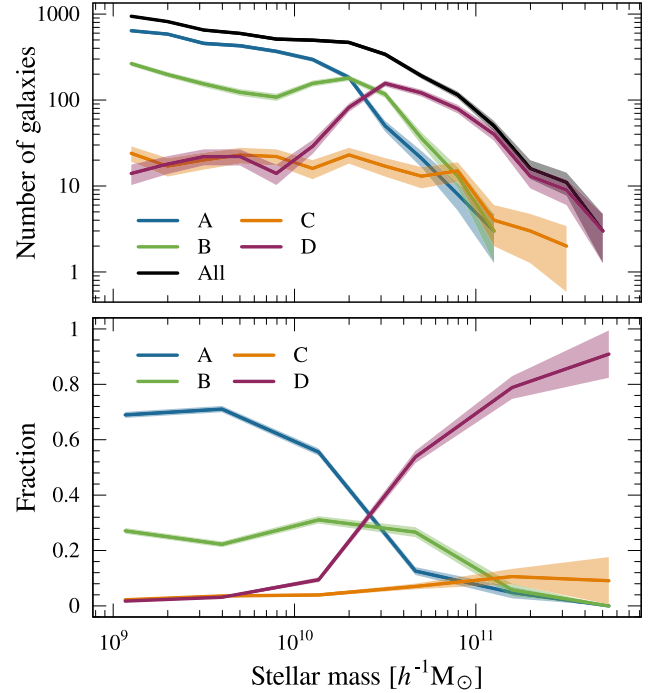


**Figure 2.** Upper panel: stellar mass distributions for the four types (colour lines) and for the complete sample (black line) of BS galaxies at  $z = 0$ . Shaded regions represent Poisson errors. Bottom panel: fractions of the four galaxy types as a function of their stellar mass at  $z = 0$ . The median values are indicated by lines, while bootstrap errors are represented by shaded regions.

the aforementioned transition value exhibit a clear manifestation of this phenomenon. To gain deeper insights into the underlying physical mechanisms responsible for the variation in the proportions of different galaxy types and their correlation with stellar mass, we analyse in detail the dynamics and astrophysical properties of these objects.

### 3 DYNAMICS

This section delves into the main aspects of the dynamics of BS galaxies, which comprises their entry and exit points from clusters, velocities, duration of the diving stage, and the proximity to the cluster centre at their pericentre. It is essential to consider not only distances with respect to the centres of clusters but also directions in space concerning the main axes of the clusters. This approach is crucial for a comprehensive understanding of the spatial orientation of objects within the cluster environment. We determine the main axes of each cluster in our sample by diagonalizing the cluster's shape tensor. For this purpose, we use the position of all galaxies whose dark matter haloes are subhaloes gravitationally bound to the main cluster halo as identified by ROCKSTAR at  $z = 0$ , that is, satellite galaxies within dark matter substructures. The shape tensor is defined as

$$S_{ij} = \sum_{k=1}^N X_k^i X_k^j, \quad (1)$$

where the dummy index  $k$  runs from 1 to the number of galaxies,  $N$ , and  $X_k^i$  and  $X_k^j$  are the  $i$ -axis and  $j$ -axis Cartesian coordinates of the galaxy  $k$ , respectively. By solving the eigenvalue problem



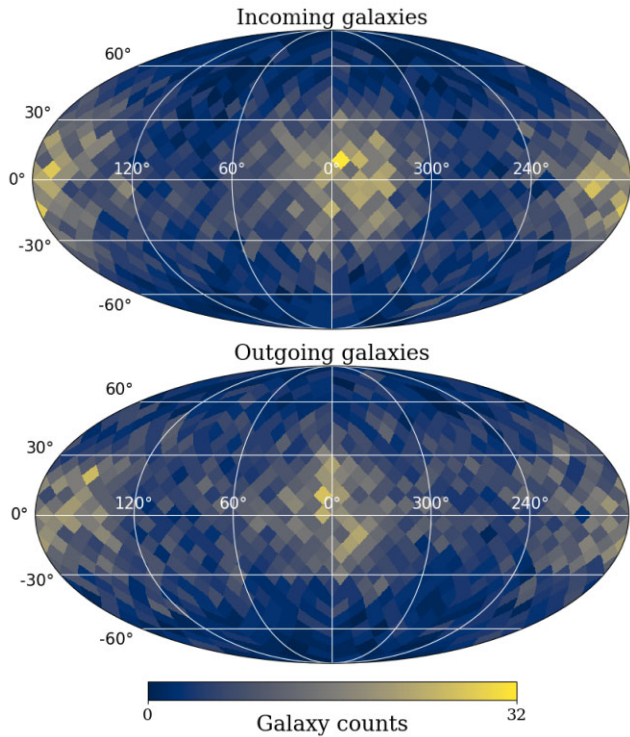


**Figure 3.** Mollweide projection of the angular distribution of galaxies relative to their parent cluster’s main axes. Upper panel: the angular distribution of incoming galaxies at the moment they cross  $R_{200}$  of the cluster in an inward direction. Lower panel: the angular distribution of outgoing galaxies as they move away from the  $R_{200}$  boundary. In these plots, the coordinates of the main axis are  $(l, b) = (0^\circ, 0^\circ)$ , and  $(180^\circ, 0^\circ)$ ; the secondary axis’ coordinates are  $(l, b) = (90^\circ, 0^\circ)$ , and  $(270^\circ, 0^\circ)$ ; the tertiary axis is located at latitude  $b = -90^\circ$ , and  $90^\circ$ .

of the shape tensor, we determine the direction of the orthogonal axes of symmetry of the galaxy distribution. The main axis will be the one along which the distribution of galaxies is most extended. The secondary and tertiary axes follow in decreasing elongation. We have computed the main axes of the clusters at many different outputs of the SAG model, and found that they are stable enough for our purposes in the last few Gyr. Thus, for simplicity, we consider the main axes at  $z = 0$  in our computations.

For each cluster, we define a right-hand rule Cartesian coordinate system where the  $X$ -axis,  $Y$ -axis, and  $Z$ -axis are the main, secondary, and tertiary axes, respectively. We define clustercentric angular positions relative to these axes taking as fundamental plane the  $X$ – $Y$  plane: the longitude  $l \in [0^\circ, 360^\circ)$ , and the latitude  $b \in [-90^\circ, 90^\circ]$ . We compute the angular position of each galaxy in our sample relative to its parent cluster and stack them all into a unique sample we use throughout the paper.

We show in Fig. 3 the stacked angular positions of galaxies when they enter their parent cluster and when they leave it (upper and lower panels, respectively). In both cases, there is a noticeable accumulation of galaxies around the primary axis. However, when galaxies enter the cluster, there appears to be a stronger concentration that tends to diffuse primarily over the  $X$ – $Y$  plane as they depart. To quantify this, we compute the angular overdensity of galaxies at the times they cross  $R_{200}$ ,

$$\Delta(\lambda, \beta) = \frac{N(\lambda, \beta)}{N_R(\lambda, \beta)} - 1, \quad (2)$$

by counting the number,  $N(\lambda, \beta)$ , of galaxies with angles

$$\lambda = \begin{cases} l, & \text{if } l \leq 90^\circ, \\ |180^\circ - l|, & \text{if } 90^\circ < l < 270^\circ, \\ 360^\circ - l, & \text{if } l \geq 270^\circ, \end{cases} \quad (3)$$

and

$$\beta = |b|. \quad (4)$$

These angles are the distance in longitude with respect to the cluster’s main axes, and the distance in latitude from the cluster’s main plane.  $N_R(\lambda, \beta)$  is the expected number of points with angular coordinates  $(\lambda, \beta)$  in a homogeneous angular distribution over the sphere. To compute this number, we generate a random distribution of angular points, which covers the sphere homogeneously. This distribution contains 100 times the number of galaxies in the sample; therefore,  $N_R(\lambda, \beta)$  is the number of these random points with coordinates  $(\lambda, \beta)$  divided by 100. In addition, we compute the overdensity of galaxies,  $\omega(\theta)$ , as a function of the angular distance to the main axis,  $\theta = \arccos(\cos(\beta) \cos(\lambda))$ , which is computed in an analogous way as  $\Delta(\lambda, \beta)$ .

The results of the computation of the angular overdensity for the general population of galaxies are shown in Fig. 4. The left-hand panel of this figure shows that the majority of galaxies tend to enter the cluster within a range of  $\sim 35^\circ$  of the plane, with some entering up to  $\sim 50^\circ$  in longitude; a strong concentration is observed towards the primary axis itself. The overdensity isocontours are found to extend farther in longitude than in latitude, with a difference of a factor  $\sim 2$  for the two highest value isocontours shown ( $\Delta = 1$  and  $1.5$ ). For outgoing galaxies (central panel), changes in the shape of the isocontours are observed, with the highest overdensity isocontours ( $\Delta \geq 0.5$ ) appearing to shrink. However, the overall overdensity enclosed by the  $\Delta = 0$  isocontour is found to extend further over the main plane, with a range of up to  $\lambda \sim 60^\circ$ . The majority of galaxies tend to enter the cluster near the primary axis and over the main plane, and to exit the cluster over the same plane, albeit with less concentration towards the primary axis. The right-hand panel of Fig. 4 reinforces this behaviour: while the overdensities of both incoming and outgoing galaxies are seen at angular scales of  $\theta \lesssim 50^\circ$ , the overdensities of incoming galaxies are systematically greater over that range. This deflection is in qualitative agreement with the results by Kuchner et al. (2022) where the authors suggest that BS galaxies entering through a filament do not necessarily return along a filament.

We perform the same analysis for the subsamples of galaxies of different types, as defined in the previous section. This is shown in Fig. 5. Each row in this figure considers a different galaxy type, from A to D, moving from top to bottom, respectively. Comprising 58 percent of the total sample, type A galaxies show angular overdensities that resemble those of the entire sample, i.e. they are mildly deflected over the main plane. Type B galaxies constitute the most interesting case, as they also display deflections over the main plane, but their trajectory out of the cluster systematically deviates from the primary axis. This is further highlighted by the characteristics exhibited in the angular overdensity  $\omega(\theta)$ : outgoing type B galaxies present a broad peak at  $15^\circ \lesssim \theta \lesssim 35^\circ$ , and a sharp decline towards  $\theta = 0^\circ$ . This strong deflection is not seen for the other three types. Finally, the less numerous type C and D galaxies seem to get in and out of the cluster much more closer to the primary axis, as if they were accreted into the cluster by inner regions of filaments and expelled out of the cluster in a similar way (González & Padilla 2016; Salerno, Martínez & Muriel

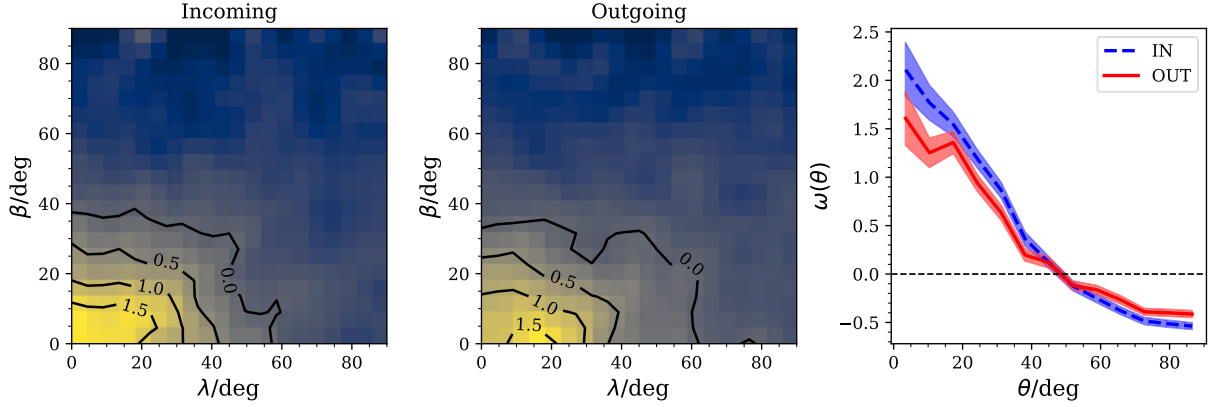


**Figure 4.** Angular overdensity of galaxies relative to their parent cluster’s main axes. Left-hand panel: overdensity of incoming galaxies as they enter  $R_{200}$  as a function of the distance in longitude with respect to the primary axis,  $\lambda$ , and the absolute value of latitude,  $\beta$ . In this plot, the primary axis of the cluster has coordinates  $(\lambda, \beta) = (0^\circ, 0^\circ)$ , the secondary  $(\lambda, \beta) = (90^\circ, 0^\circ)$ , and the tertiary  $\beta = 90^\circ$ . Some relevant isocontours are drawn in solid line. Middle panel: same as the left-hand panel but for outgoing galaxies. Right-hand panel: the angular overdensity of incoming (IN) and outgoing (OUT) galaxies as a function of the angular distance,  $\theta$ , to the primary cluster axis. Errors are computed using the bootstrap resampling technique.

2019; Morinaga & Ishiyama 2020; Salerno et al. 2020). This is consistent with the definition of these two types, they are either already quenched when they enter the cluster, or are quenched in their incursion through it.

Other dynamical parameters are shown in Fig. 6, namely incoming velocity, the distance of the pericentre, the time span of the diving stage, the ratio between the incoming and the outgoing velocities, and the time span of the backplash stage. All these parameters are shown as median values per type, as a function of stellar mass (left-hand panels), and as a single value stacking all galaxies together regardless of their mass (right-hand panel). It is evident from the left-hand panels that there are no notable patterns between these parameters and stellar mass and, also, it is fair to notice the lack of some types of galaxies for stellar masses higher than  $\sim 7 \times 10^{10} h^{-1} M_\odot$ , where a complete comparison cannot be done.

Regarding the incoming velocity (top panels), it seems that type C galaxies have a tendency to enter clusters at lower velocities compared to the other types, whereas no discernible difference is observed among types A, B, and D. Instead, in the case of pericentre distance (shown in the second panel from the top), type A galaxies stand out, as they exhibit systematically larger distances from the cluster centre at their closest point to it than the other galaxy types. On the other hand, there are no significant differences among the other types. When analysing how long galaxies are inside  $R_{200}$  (middle panels), we find that types A and D cannot be distinguished, but type B spends the least amount of time, while on the opposite end, type C remains for the longest duration. There is no difference among the four types with regards to the ratio between the outgoing and incoming velocities (second panel from the bottom). All types get out of the cluster at speeds  $\sim 20$  per cent lower than they had when they entered the cluster. Finally, type B galaxies are the ones that have spent the longest time in the backplash stage, while no differences are seen among the other types (bottom panel).

We have checked that 27 per cent of the complete sample of BS galaxies are falling back to the cluster at  $z = 0$ , and this fraction does not vary significantly with the galaxy type. The only exception are type B galaxies for which this percentage increases to 38, in consistency with the fact that they spend typically longer times in the backplash stage.

## 4 THE PHYSICAL EVOLUTION OF BACKSPASH GALAXIES

In this section, we study how physical properties of MDPL2-SAG BS galaxies evolve in the three stages. We focus on some quantities provided by the SAG model: stellar mass, dark matter halo mass, cold gas mass, hot gas mass, and the sSFR. Towards the end of this section, we examine morphological changes experienced by these galaxies by using the ratio of bulge mass to total stellar mass as a proxy of morphology.

### 4.1 Astrophysical quantities

The evolution of astrophysical properties of BS galaxies is presented in Fig. 7. As temporal variable we use  $\tau$ , defined as the time a galaxy remains in a particular stage conveniently normalized. For the incoming stage, we considered as  $\tau = 0$  to 2Gyr the time before the galaxy crosses  $R_{200}$  inwards the cluster, and  $\tau = 1$  as the moment when the galaxy crosses  $R_{200}$  for the first time. For the diving stage,  $\tau = 0$  is set as the moment the galaxy crosses  $R_{200}$  inwards the cluster and  $\tau = 1$  when the galaxy crosses  $R_{200}$  outwards. Finally, in the backplash stage, we define as  $\tau = 0$  the time the galaxy crosses  $R_{200}$  for the second time and  $\tau = 1$  corresponds to  $z = 0$ . With this normalized time, we stacked the evolution of astrophysical properties normalized to their values at a particular moment  $\tau_*$ : this  $\tau_*$  is the first crossing of  $R_{200}$  for incoming and diving stages, and corresponds to the second crossing of  $R_{200}$  for the backplash stage. All these time definitions are shown in the bottom panels of the figure. From top to bottom in Fig. 7, the properties shown are stellar mass, dark matter halo mass, cold gas mass, hot gas mass, and sSFR. In all cases, we show the median values of the evolution of the stacked galaxy population with error bars (shaded regions) computed with a bootstrap resampling.

We begin our analysis by studying the total stellar mass of galaxies. Type A galaxies exhibit the most substantial increase in their stellar masses across the three stages: approximately 20 per cent during the incoming stage, 10 per cent during the diving stage, and 5 per cent during the backplash stage. Type B galaxies show a similar trend during the first two stages, but their median growth in stellar mass halts during the backplash stage. This outcome

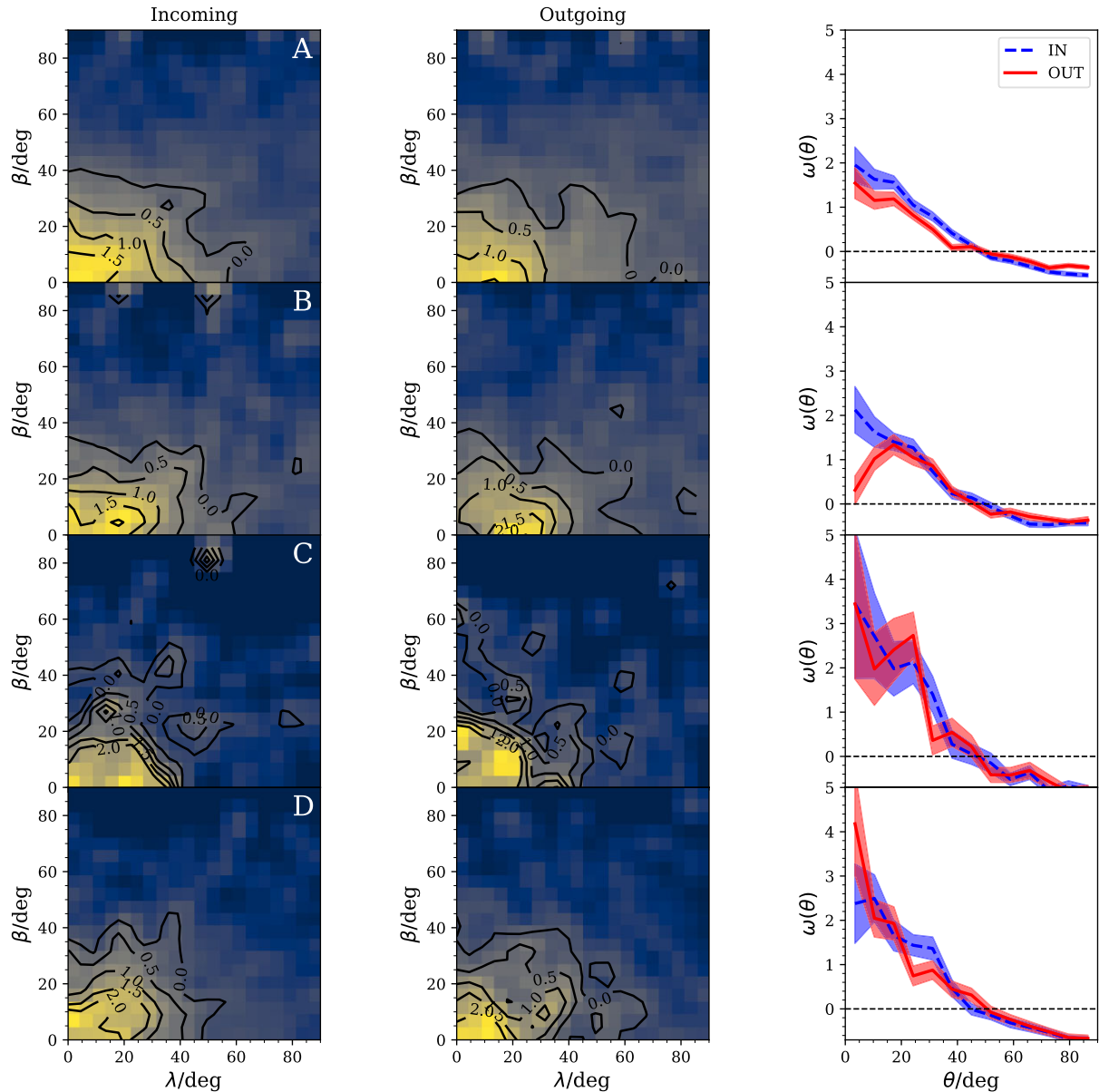


**Figure 5.** Same as Fig. 4 but considering each of the four types of galaxies separately as quoted in left-hand panels.

is anticipated since, by definition, these galaxies become passive during this stage. In the case of type C and D galaxies, only type C galaxies exhibit a marginal increase of  $\sim 5$  per cent in their masses during the incoming stage. These behaviours are consistent with our classification: galaxies that become passive at a later stage exhibit a correspondingly delayed decrease in the median stellar mass growth.

The evolution of the mass of the dark matter halo where the galaxy resides is completely determined by the dynamical interactions of the haloes across their merger tree histories. As can be seen in the second row of panels from Fig. 7, for all galaxy types, the host haloes decrease in mass across the three stages. In the incoming stage, haloes of type C galaxies are the most affected, losing up to  $\sim 20$  per cent of their mass. Similarly, the diving stage causes a more significant impact on the haloes of type C galaxies ( $\sim 40$  per cent), whereas the haloes of the remaining types experience losses of around 20 per cent. The fact that type C galaxies become passive during the diving stage

may be correlated with the significant mass disruption experienced by their host haloes during this stage. This tidal stripping of their haloes exposes them to a stronger effect of the ram pressure upon their hot gas (see Vega-Martínez et al. 2022 for details of the implementation of these processes in SAG). Furthermore, these galaxies endured heavy pre-processing in the incoming stage. During the backplash stage, haloes of type B galaxies are those that experience the greatest impact on their masses, with a decrease of over  $\sim 40$  per cent. Nevertheless, haloes of the other galaxy types also show a reduction of  $\sim 30$  per cent in their masses at  $z = 0$ . Once again, we notice a correlation between the haloes that suffer the most significant mass-loss and the fact that the galaxies inhabiting them (type B) become passive during this stage. This finding is consistent with their null stellar mass growth. It is worth noting that, during the backplash stage, all galaxies except for type A have ceased to grow their stellar mass, and the dark matter haloes continue to shrink across all classifications.

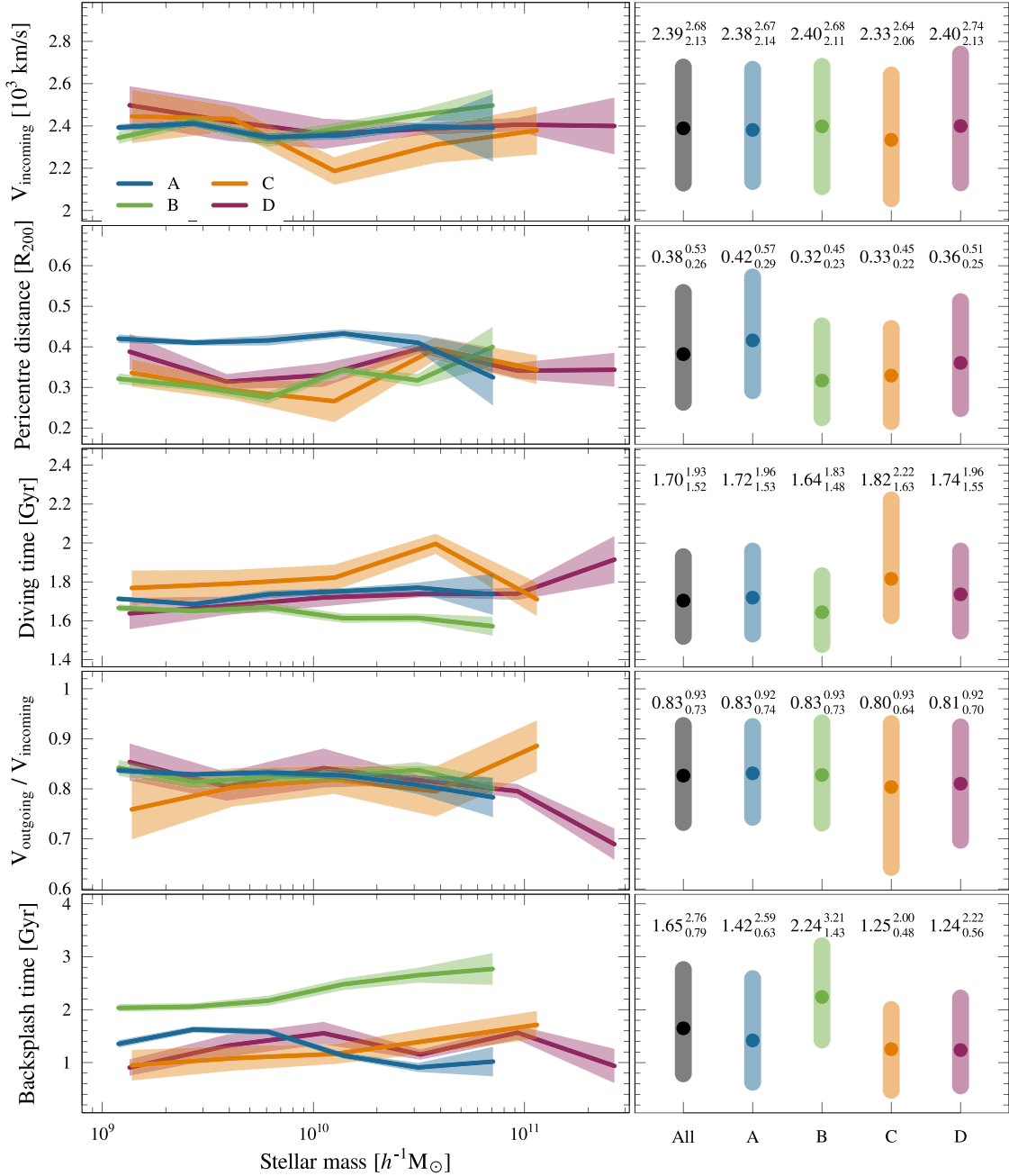


**Figure 6.** Left-hand panels: dependence of several dynamical properties with stellar mass for the four types of galaxies. From top to bottom: incoming velocity modulus, normalized pericentre distance, time in the diving stage, ratio between outgoing and incoming velocity modulus, and time in the backsplash stage. In all cases, we show the median value and the errors computed with bootstrap resampling. Right-hand panels: median values (central dot) and quartiles (shaded bars) for the same properties described in left-hand panels. Numerical values are quoted for each type, including the complete sample of galaxies.

In the third and fourth rows of panels of Fig. 7, we show the evolution of the cold and hot gas masses, respectively. Type A galaxies do not undergo significant changes in their cold and hot gas masses during the incoming stage, but suffer a reduction of  $\sim 20$  percent of the cold gas and  $\sim 50$  percent of the hot gas when they are located inside the  $R_{200}$  radius of the cluster. Once they are out, in the backsplash stage, they continue losing cold gas ( $\sim 30$  percent) but the amount of hot gas remains stable. This may be explained by the negligible effect of the RPS on these galaxies due to their greater distance from the cluster. Type B galaxies

lose more than 50 percent of their cold gas during the backsplash stage, period where these galaxies become passive. They also get their hot gas drastically removed in the diving ( $\sim 50$  percent) and backsplash ( $\sim 40$  percent) stages. Notably, the difference between type B and type A galaxies is that in the backsplash stage, type B galaxies experience a considerable removal of hot gas, while type A galaxies retain their hot gas. This difference explains why type B galaxies become passive during the backsplash stage. In the incoming stage, type C galaxies suffer a large reduction of  $\sim 70$  percent in their cold gas mass, which continues during the



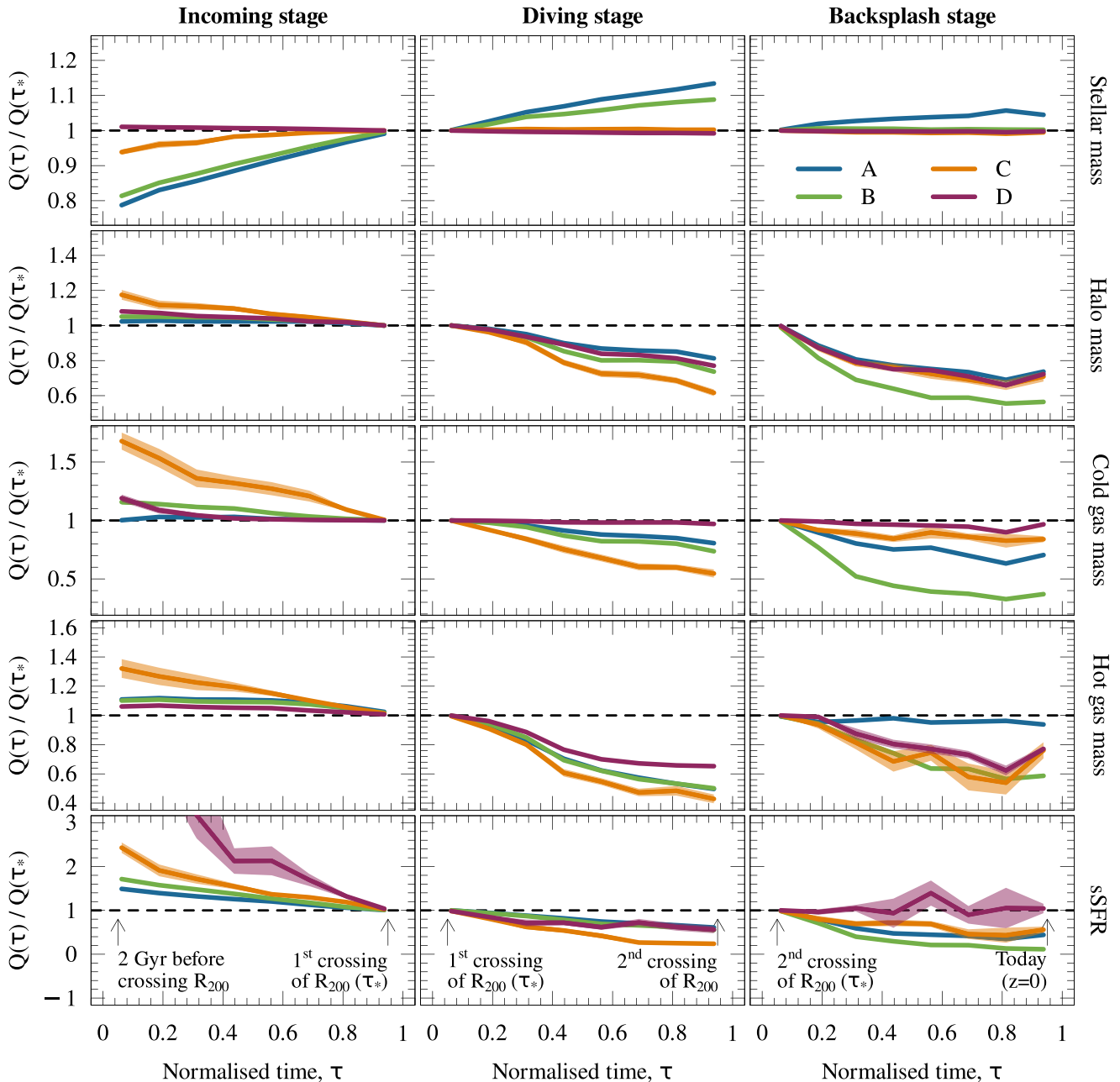


**Figure 7.** Evolution of normalized astrophysical properties for the four types of galaxies in the three stages. Evolution is parametrized with  $\tau$ , a normalized time at two particular moments in each stage, as indicated with arrows in the bottom panels. The astrophysical properties are normalized at their values at  $\tau_*$ , which is the first crossing of  $R_{200}$  for the incoming and diving stages, and the second crossing of  $R_{200}$  for the backsplash stage. Properties  $Q$  are, from top to bottom, the stellar mass, the dark matter halo mass, the mass in cold gas, the mass in hot gas, and the sSFR. In all cases, we show the median of the stacked galaxy population and error bars computed via bootstrap resampling.

diving stage, reaching another reduction of  $\sim 50$  percent at the time the galaxy leaves the cluster. The same occurs with hot gas, suffering reductions of  $\sim 30$ ,  $60$ , and  $40$  per cent during the incoming, diving, and backsplash stages, respectively. Type D galaxies exhibit a notable change in their cold gas content only during the initial phase of the incoming stage, which is in line with their quenched state upon entering the cluster. At this point, the cold gas is neither consumed by star formation nor removed by RPS, as these galaxies still possess a hot gas shield that is gradually stripped

away, reaching a loss of  $\sim 35$  per cent in the diving and backsplash stages.

Finally, in the last row we show the sSFR. While all galaxy types exhibit a decrease in their sSFR throughout all stages, it is evident that type D galaxies, which are already passive upon infalling into the cluster, are highly affected during the incoming stage. These galaxies experience a further decrease in their sSFR during the diving stage and maintain a stable sSFR during the backsplash stage. Type C galaxies also experience a significant

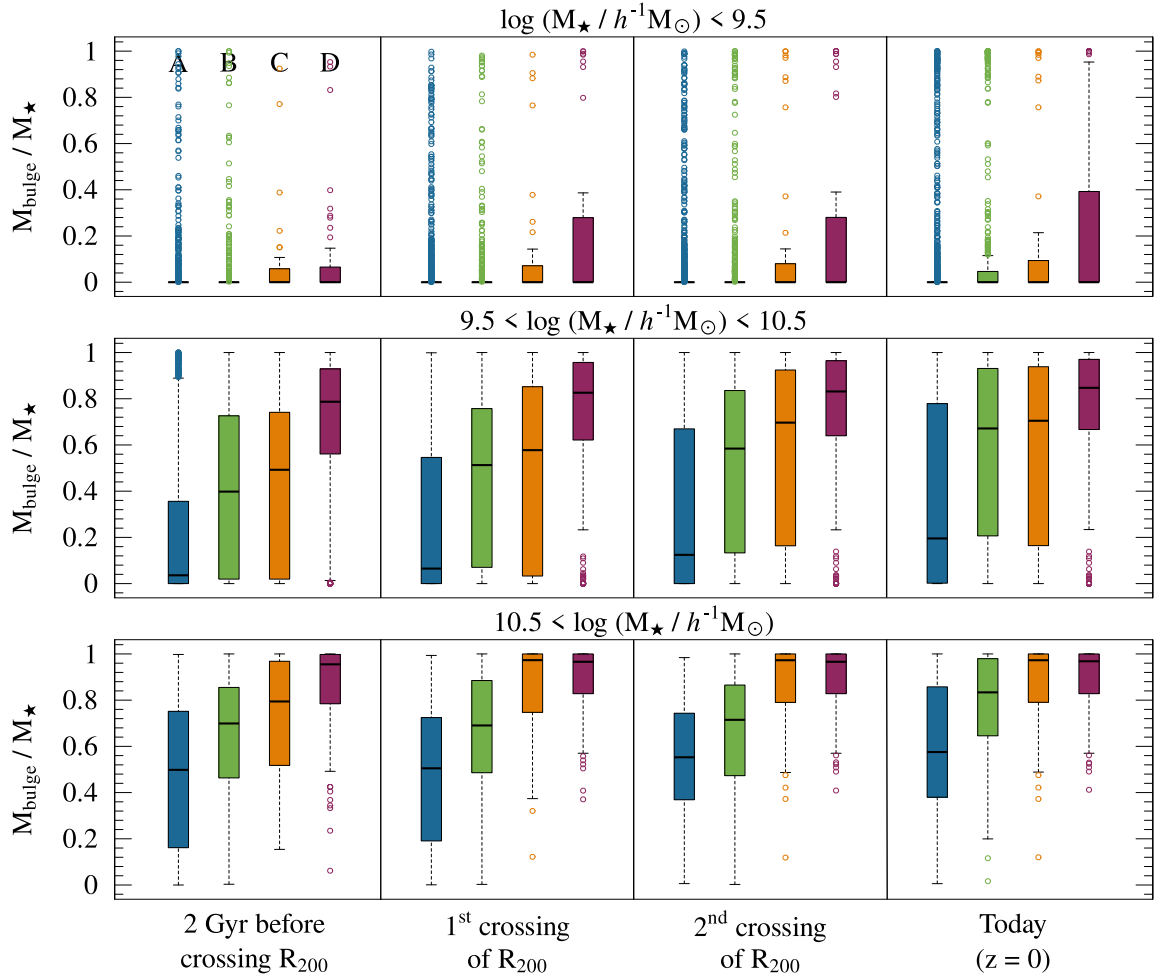


**Figure 8.** Boxplots for morphological distributions for the four galaxy types, where morphology is defined as the ratio between the bulge mass and the total stellar mass,  $M_{\text{bulge}}/M_{\star}$ . Distributions are shown for three stellar mass cuts, from low-mass galaxies (top) to high-mass galaxies (bottom), and at four different moments in the galaxy’s lifetime, as indicated in the  $x$ -axis labels. In each boxplot, the colour bar represents the interquartile range  $\text{IQR} = Q_3 - Q_1$ , where  $Q_1$  and  $Q_3$  are the first and third quartiles of the distribution, respectively, and the median value is shown with the short horizontal black line. The dashed vertical lines show the range covered by the minimum and maximum values, without considering the outliers of the distribution, which are defined as those at a distance greater than  $1.5 \times \text{IQR}$  of  $Q_1$  or  $Q_3$  and symbolized with the coloured open circles.

drop in their sSFR during the incoming stage, and they are the most affected among all types in the diving stage, losing nearly all their ability to form stars. During the incoming and diving stages, types A and B exhibit similar trends by reducing their sSFR by  $\sim 50$ . However, in the backplash stage, type B galaxies become passive and experience the most significant decrease in sSFR.

#### 4.2 Morphology

The overall analysis of the sSFR fails to distinguish between the two modes of star formation: quiescent and bursty. In the context of SAG, generally considered in galaxy formation models, quiescent star formation contributes to the creation of the stellar disc, while bursty star formation, triggered by mergers and disc instabilities, leads to the formation of the stellar bulge. The proportion of the galaxy’s total stellar mass that the bulge represents is an indicator of the galaxy’s morphology.

In this section, we analyse how the morphology of galaxies evolves across the three stages. To do this, we define as a proxy of the

morphology the ratio of the bulge mass to the total stellar mass,  $M_{\text{bulge}}/M_{\star}$ . This ratio ranges between 0 for irregular galaxies (no bulge mass) and 1 for elliptical galaxies (no disc mass), with spiral galaxies between those two extreme values.

In Fig. 8, we present boxplots for morphology distributions at four fixed times, from left to right: 2 Gyr before the galaxy crosses  $R_{200}$  for the first time, the moment when the galaxy crosses  $R_{200}$  inwards, the moment when the galaxy crosses  $R_{200}$  outwards, and the present time ( $z = 0$ ). Also, we divide the samples of galaxy types into three stellar mass ranges, from top to bottom:  $\log(M_{\star}/h^{-1} M_{\odot}) < 9.5$  (low mass),  $9.5 < \log(M_{\star}/h^{-1} M_{\odot}) < 10.5$  (intermediate mass), and  $10.5 < \log(M_{\star}/h^{-1} M_{\odot})$  (high mass).

The first feature easily noticeable is that, at early times, low-mass galaxies (top panels) mostly have  $M_{\text{bulge}}/M_{\star} \sim 0$ , which does not change significantly across the galaxy’s lifetime. In particular, type A and B populations are highly dominated by bulgeless galaxies, which represent 90, 84, 81, and 79 per cent of the sample for type A, and 85, 79, 75, and 71 per cent of the sample for type B, at each of the moments considered along the galaxy’s lifetime. Only type D galaxies show a mild evolution in their morphology, especially

between the 2 Gyr before entering the cluster and the moment galaxies cross  $R_{200}$  for the first time, that is, during the incoming stage. For intermediate and high stellar masses (middle and bottom panels, respectively), we can appreciate a smooth morphological change across cosmic time for all galaxy types.

These results show that the morphological evolution of galaxies is a smooth and continuous process during the stages defined in this work. We do not find evidence that a particular moment in the lifetime of BS galaxies can induce a major morphological transformation, in agreement with Martínez et al. (2023), where the authors find evidence that quenching occurs faster than morphological transformation for galaxies around massive X-ray clusters as classified with ROGER (de los Rios et al. 2021). We only find a clear dependence of morphology with the stellar mass cuts analysed, dependence that is also manifested through the relationship between the galaxy type and its stellar mass (see Fig. 2). At this point, it is worth recalling that larger stellar masses correlate with larger bulge masses, and this implies the existence of larger black holes in those galaxies (Kormendy & Ho 2013; McConnell & Ma 2013; Schutte, Reines & Greene 2019). These massive black holes bring with them an associated major feedback from active galactic nuclei that accelerates the quenching processes, especially for types C and D.

## 5 CONCLUSIONS

In this paper, we have studied the population of BS galaxies around a sample of massive, isolated clusters at  $z = 0$  in the MDPL2-SAG catalogue of simulated galaxies. It is important to recall that our definition of BS galaxy involves a single passage within  $R_{200}$ ; thus, these galaxies experience the environmental action of the cluster only in this single passage. The main focus of this paper is to understand what happens to a galaxy that passes only once through a cluster, and not the cumulative effect of several orbits inside the cluster. We classified the BS galaxies into four types based on their star-forming or passive nature at three different stages: incoming stage, diving stage, and backsplash stage. We analysed various dynamical and astrophysical properties of these galaxies.

For galaxies that are actively forming stars at all stages (type A), we find that they typically have stellar masses below  $3 \times 10^{10} h^{-1} M_{\odot}$  at  $z = 0$ . Due to their orbits avoiding the innermost regions of the cluster, their incursion into the cluster has minimal impact on them. Consequently, they do not experience significant losses in their dark matter or gas contents, allowing them to continue forming stars.

We find that BS galaxies that become passive during the backsplash stage (type B) also have masses typically below  $3 \times 10^{10} h^{-1} M_{\odot}$  at  $z = 0$ , similar to type A galaxies. They constitute the vast majority of passive BS galaxies in that mass range. Their orbits inside the cluster are characterized by the smallest pericentric distances of all four types, and, on average, they experience a strong deflection away from the primary axes in their way out. This close encounter with the centre of the cluster is the single most important factor in the subsequent evolution of these galaxies. The action of the cluster leaves its mark in the strong loss of these galaxies' dark matter and gas contents, and the subsequent suppression of their star formation in the backsplash stage. Had these galaxies not come that close to the centre, they would probably have been classified as type A. This galaxy population can be associated with the low-mass galaxies quenched after their first passage through the pericentre in massive clusters described by Wright et al. (2022) using the EAGLE simulations (Crain et al. 2015; Schaye et al. 2015).

Regarding those galaxies that become passive during the diving stage (type C), they are the least abundant among all BS galaxies.

They entered the cluster in close proximity to the primary axes and underwent significant pre-processing. Among the galaxies that enter the cluster while still forming stars, these galaxies are the ones that remain for the longest duration and endure the greatest reductions in their dark matter and gas contents in the incoming stage. The cluster then provides the final blow to these galaxies' star formation.

Finally, galaxies that are passive throughout the three stages (type D) are typically high-mass galaxies that were quenched before entering the cluster. Typically, they are accreted close to the primary axes, and get out of the cluster along the same axes. There is nothing particularly noteworthy about these galaxies after they dive into the cluster.

Our results are in agreement with those presented by Hough et al. (2023), where the authors show that 65 per cent of present-day star-forming BS galaxies did not experience pre-processing effects before their passage to the pericentre. On the other hand, 70 per cent of  $z = 0$  quenched galaxies suffer larger removals of hot gas during their pre-processing instances (incoming stage) and inside the cluster (diving stage). These quenched BS galaxies can be clearly related with our D and C types, respectively. It is important to mention that the authors define as BS a galaxy that is outside  $R_{200}$  at  $z = 0$  but has been inside the cluster at least once in the past, which is slightly different from our definition, where we allow just one passage to the pericentre. This difference implies that some of their BS galaxies should be more quenched than ours as they have suffered the action of the cluster in more than one passage.

Regarding morphology, a consistent pattern is observed across the four types: a single passage through the cluster does not generally induce significant morphological transformations, as suggested by Martínez et al. (2023). It should be kept in mind that we are using a proxy for morphology and not a precise characterization of it.

The main result of this paper is that the environmental effects of the cluster are able to affect galaxies after a single passage provided they are either low- to intermediate-mass ( $< 3 \times 10^{10} h^{-1} M_{\odot}$ ) galaxies whose orbits take them very close to the centre or galaxies that entered the cluster heavily pre-processed. The former stop forming stars after exiting the cluster, while the latter do so *in situ*.

## ACKNOWLEDGEMENTS

We kindly thank the anonymous referee for comments and suggestions that improved the original manuscript. This paper has been partially supported with grants from Consejo Nacional de Investigaciones Científicas y Técnicas, Argentina (PIPs 11220130100365CO, 11220210100064CO, and 11220200102832CO), the Agencia Nacional de Promoción Científica y Tecnológica, Argentina (PICTs 2018-3743, 2020-3690 and 2021-I-A-00700), and Secretaría de Ciencia y Tecnología, Universidad Nacional de Córdoba, Argentina. ANR thanks the Scaloneta for winning the 2022 FIFA World Cup. SAC acknowledges funding from CONICET (PIP-2876) and the Universidad Nacional de La Plata (G11-150). MdIR acknowledges financial support from the Comunidad Autónoma de Madrid through the grant SI2/PBG/2020-00005. The CosmoSim data base used in this paper is a service by the Leibniz-Institute for Astrophysics Potsdam (AIP). The MultiDark data base was developed in cooperation with the Spanish MultiDark Consolider Project CSD2009-00064. The authors gratefully acknowledge the Gauss Centre for Supercomputing e.V. ([www.gauss-centre.eu](http://www.gauss-centre.eu)) and the Partnership for Advanced Supercomputing in Europe (PRACE; [www.prace-ri.eu](http://www.prace-ri.eu)) for funding the MULTIDARK simulation project by providing computing time on the GCS Supercomputer SuperMUC at Leibniz Supercomputing Centre (LRZ; [www.lrz.de](http://www.lrz.de)). All analyses in this paper have been done using

the FORTRAN language (<https://fortran-lang.org>), and figures have been developed using R (R Core Team 2021), MATPLOTLIB (Hunter 2007), HEALPIX/HEALPY (Górski et al. 2005; Zonca et al. 2019), and INKSCAPE (<https://inkscape.org>).

## DATA AVAILABILITY

The raw data of the semi-analytical model of galaxy formation SAG will be shared on reasonable request to the corresponding author.

## REFERENCES

- Abadi M. G., Moore B., Bower R. G., 1999, *MNRAS*, 308, 947
- Adami C., Biviano A., Mazure A., 1998, *A&A*, 331, 439
- Aguerri J. A. L., Sánchez-Janssen R., 2010, *A&A*, 521, A28
- Bahé Y. M., McCarthy I. G., Balogh M. L., Font A. S., 2013, *MNRAS*, 430, 3017
- Balogh M. L., Navarro J. F., Morris S. L., 2000, *ApJ*, 540, 113
- Bamford S. P. et al., 2009, *MNRAS*, 393, 1324
- Barnes J. E., 1992, *ApJ*, 393, 484
- Behroozi P. S., Wechsler R. H., Wu H.-Y., 2013a, *ApJ*, 762, 109
- Behroozi P. S., Wechsler R. H., Wu H.-Y., Busha M. T., Klypin A. A., Primack J. R., 2013b, *ApJ*, 763, 18
- Behroozi P. S., Wechsler R. H., Lu Y., Hahn O., Busha M. T., Klypin A., Primack J. R., 2014, *ApJ*, 787, 156
- Bekki K., 2009, *MNRAS*, 399, 2221
- Benavides J. A. et al., 2021, *Nat. Astron.*, 5, 1255
- Berrier J. C., Stewart K. R., Bullock J. S., Purcell C. W., Barton E. J., Wechsler R. H., 2009, *ApJ*, 690, 1292
- Blanton M. R., Moustakas J., 2009, *ARA&A*, 47, 159
- Blanton M. R., Eisenstein D., Hogg D. W., Schlegel D. J., Brinkmann J., 2005, *ApJ*, 629, 143
- Book L. G., Benson A. J., 2010, *ApJ*, 716, 810
- Borrow J., Vogelsberger M., O’Neil S., McDonald M. A., Smith A., 2023, *MNRAS*, 520, 649
- Bower R. G., Benson A. J., Crain R. A., 2012, *MNRAS*, 422, 2816
- Casey K. J., Greco J. P., Peter A. H. G., Davis A. B., 2023, *MNRAS*, 520, 4715
- Christensen C. R., Davé R., Governato F., Pontzen A., Brooks A., Munshi F., Quinn T., Wadsley J., 2016, *ApJ*, 824, 57
- Cimatti A. et al., 2013, *ApJ*, 779, L13
- Coenda V., Muriel H., Donzelli C. J., Quintana H., Infante L., García Lambas D., 2006, *AJ*, 131, 1989
- Coenda V., Mast D., Martínez H. J., Muriel H., Merchán M. E., 2019, *A&A*, 621, A98
- Coenda V., de los Rios M., Muriel H., Cora S. A., Martínez H. J., Ruiz A. N., Vega-Martínez C. A., 2022, *MNRAS*, 510, 1934
- Colberg J. M., White S. D. M., Jenkins A., Pearce F. R., 1999, *MNRAS*, 308, 593
- Cooper M. C., Gallazzi A., Newman J. A., Yan R., 2010, *MNRAS*, 402, 1942
- Cora S. A. et al., 2018, *MNRAS*, 479, 2
- Crain R. A. et al., 2015, *MNRAS*, 450, 1937
- Cui W. et al., 2018, *MNRAS*, 480, 2898
- Dalla Vecchia C., Schaye J., 2008, *MNRAS*, 387, 1431
- de los Rios M., Martínez H. J., Coenda V., Muriel H., Ruiz A. N., Vega-Martínez C. A., Cora S. A., 2021, *MNRAS*, 500, 1784
- De Lucia G., Weinmann S., Poggianti B. M., Aragón-Salamanca A., Zaritsky D., 2012, *MNRAS*, 423, 1277
- Delfino F. M., Scóccola C. G., Cora S. A., Vega-Martínez C. A., Gargiulo I. D., 2022, *MNRAS*, 510, 2900
- Di Matteo P., Combes F., Melchior A. L., Semelin B., 2007, *A&A*, 468, 61
- Domínguez M., Muriel H., Lambas D. G., 2001, *AJ*, 121, 1266
- Dressler A., 1980, *ApJ*, 236, 351
- Ebeling H., Barrett E., Donovan D., 2004, *ApJ*, 609, L49
- Fujita Y., 2004, *PASJ*, 56, 29
- Gill S. P. D., Knebe A., Gibson B. K., 2005, *MNRAS*, 356, 1327
- Gnedin O. Y., 2003a, *ApJ*, 582, 141
- Gnedin O. Y., 2003b, *ApJ*, 589, 752
- González R. E., Padilla N. D., 2016, *ApJ*, 829, 58
- Górski K. M., Hivon E., Banday A. J., Wandelt B. D., Hansen F. K., Reinecke M., Bartelmann M., 2005, *ApJ*, 622, 759
- Gunn J. E., Gott J. R. I., 1972, *ApJ*, 176, 1
- Haggard R., Gray M. E., Pearce F. R., Knebe A., Cui W., Mostoghiu R., Yepes G., 2020, *MNRAS*, 492, 6074
- Hashimoto Y., Oemler A., Jr, Lin H., Tucker D. L., 1998, *ApJ*, 499, 589
- Hasinger G., 2008, *A&A*, 490, 905
- Hopkins P. F., Quataert E., Murray N., 2012, *MNRAS*, 421, 3522
- Hou A., Parker L. C., Harris W. E., 2014, *MNRAS*, 442, 406
- Hough T. et al., 2023, *MNRAS*, 518, 2398
- Hunter J. D., 2007, *Comput. Sci. Eng.*, 9, 90
- Jackson R. A., Kaviraj S., Martin G., Devriendt J. E. G., Noakes-Kettel E. A., Silk J., Ogle P., Dubois Y., 2022, *MNRAS*, 511, 607
- Klypin A., Yepes G., Gottlöber S., Prada F., Heß S., 2016, *MNRAS*, 457, 4340
- Knebe A. et al., 2018, *MNRAS*, 474, 5206
- Knebe A. et al., 2020, *MNRAS*, 495, 3002
- Kormendy J., Ho L. C., 2013, *ARA&A*, 51, 511
- Kuchner U. et al., 2022, *MNRAS*, 510, 581
- Larson R. B., Tinsley B. M., Caldwell C. N., 1980, *ApJ*, 237, 692
- Lu T., Gilbank D. G., McGee S. L., Balogh M. L., Gallagher S., 2012, *MNRAS*, 420, 126
- Mamon G. A., Sanchis T., Salvador-Solé E., Solanes J. M., 2004, *A&A*, 414, 445
- Marinacci F. et al., 2018, *MNRAS*, 480, 5113
- Martin G., Kaviraj S., Devriendt J. E. G., Dubois Y., Pichon C., 2018, *MNRAS*, 480, 2266
- Martínez H. J., Muriel H., 2006, *MNRAS*, 370, 1003
- Martínez H. J., Coenda V., Muriel H., 2008, *MNRAS*, 391, 585
- Martínez H. J., Muriel H., Coenda V., 2016, *MNRAS*, 455, 127
- Martínez H. J., Coenda V., Muriel H., de los Rios M., Ruiz A. N., 2023, *MNRAS*, 519, 4360
- Mateus A., Sodré L., 2004, *MNRAS*, 349, 1251
- McCarthy I. G., Frenk C. S., Font A. S., Lacey C. G., Bower R. G., Mitchell N. L., Balogh M. L., Theuns T., 2008, *MNRAS*, 383, 593
- McConnell N. J., Ma C.-P., 2013, *ApJ*, 764, 184
- McGee S. L., Balogh M. L., Bower R. G., Font A. S., McCarthy I. G., 2009, *MNRAS*, 400, 937
- Mihos J. C., 2004, in Mulchaey J. S., Dressler A., Oemler A., eds, *Clusters of Galaxies: Volume 3, Carnegie Observatories Astrophysics Series: Probes of Cosmological Structure and Galaxy*. Cambridge Univ. Press, Cambridge, p. 277
- Moore B., Katz N., Lake G., Dressler A., Oemler A., 1996, *Nature*, 379, 613
- Moore B., Lake G., Katz N., 1998, *ApJ*, 495, 139
- Morinaga Y., Ishiyama T., 2020, *MNRAS*, 495, 502
- Muratov A. L., Kereš D., Faucher-Giguère C.-A., Hopkins P. F., Quataert E., Murray N., 2015, *MNRAS*, 454, 2691
- Muriel H., Coenda V., 2014, *A&A*, 564, A85
- Naiman J. P. et al., 2018, *MNRAS*, 477, 1206
- Nandra K. et al., 2007, *ApJ*, 660, L11
- Navarro J. F., White S. D. M., 1994, *MNRAS*, 267, 401
- Nelson D. et al., 2018, *MNRAS*, 475, 624
- Paulino-Afonso A. et al., 2019, *A&A*, 630, A57
- Pillepich A. et al., 2018, *MNRAS*, 475, 648
- Planck Collaboration XVI, 2014, *A&A*, 571, A16
- Planck Collaboration XIII, 2016, *A&A*, 594, A13
- R Core Team, 2021, *R: A Language and Environment for Statistical Computing*. R Foundation for Statistical Computing, Vienna, Austria
- Riebe K. et al., 2013, *Astron. Nachr.*, 334, 691
- Rines K., Diaferio A., 2006, *AJ*, 132, 1275
- Rost A., Stasyszyn F., Pereyra L., Martínez H. J., 2020, *MNRAS*, 493, 1936
- Ruiz A. N. et al., 2015, *ApJ*, 801, 139
- Salerno J. M., Martínez H. J., Muriel H., 2019, *MNRAS*, 484, 2
- Salerno J. M. et al., 2020, *MNRAS*, 493, 4950
- Schaefer A. L. et al., 2017, *MNRAS*, 464, 121
- Schaye J. et al., 2015, *MNRAS*, 446, 521



- Schutte Z., Reines A. E., Greene J. E., 2019, *ApJ*, 887, 245
- Silverman J. D. et al., 2008, *ApJ*, 675, 1025
- Smith R. et al., 2015, *MNRAS*, 454, 2502
- Springel V., 2005, *MNRAS*, 364, 1105
- Springel V., White S. D. M., Tormen G., Kauffmann G., 2001, *MNRAS*, 328, 726
- Springel V. et al., 2018, *MNRAS*, 475, 676
- Steinhauser D., Schindler S., Springel V., 2016, *A&A*, 591, A51
- Stringer M. J., Bower R. G., Cole S., Frenk C. S., Theuns T., 2012, *MNRAS*, 423, 1596
- Thomas D., Maraston C., Bender R., Mendes de Oliveira C., 2005, *ApJ*, 621, 673
- Toomre A., 1977, in Tinsley B. M., Larson R. B., Gehret D. C., eds, Proceedings of a Conference at Yale University, Evolution of Galaxies and Stellar Populations. Yale University Observatory, New Haven, p. 401
- Vega-Martínez C. A., Gómez F. A., Cora S. A., Hough T., 2022, *MNRAS*, 509, 701
- Vijayaraghavan R., Ricker P. M., 2015, *MNRAS*, 449, 2312
- Villalobos Á., De Lucia G., Murante G., 2014, *MNRAS*, 444, 313
- Weinmann S. M., van den Bosch F. C., Yang X., Mo H. J., 2006, *MNRAS*, 366, 2
- Welikala N., Connolly A. J., Hopkins A. M., Scranton R., Conti A., 2008, *ApJ*, 677, 970
- Wetzel A. R., Tinker J. L., Conroy C., 2012, *MNRAS*, 424, 232
- Wetzel A. R., Tinker J. L., Conroy C., van den Bosch F. C., 2013, *MNRAS*, 432, 336
- Whitmore B. C., Gilmore D. M., Jones C., 1993, *ApJ*, 407, 489
- Wright R. J., Lagos C. d. P., Power C., Stevens A. R. H., Cortese L., Poulton R. J. J., 2022, *MNRAS*, 516, 2891
- Zheng Z. et al., 2017, *MNRAS*, 465, 4572
- Zonca A., Singer L., Lenz D., Reinecke M., Rosset C., Hivon E., Gorski K., 2019, *J. Open Source Softw.*, 4, 1298
- Zwicky F., 1951, *PASP*, 63, 17

This paper has been typeset from a  $\text{\TeX}/\text{\LaTeX}$  file prepared by the author.